New statistical scission-point model to predict fission fragment observables

Jean-François Lemaître
CEA Centre de Saclay, Irfu/Service de Physique Nucléaire, F-91191, Gif-sur-Yvette, France
and CEA, DAM, DIF, F-91297, Arpajon, France

Stefano Panebianco and Jean-Luc Sida
CEA Centre de Saclay, Irfu/Service de Physique Nucléaire, F-91191, Gif-sur-Yvette, France

Stéphane Hilaire and Sophie Heinrich*
CEA, DAM, DIF, F-91297, Arpajon, France
(Received 26 January 2015; revised manuscript received 23 May 2015; published 28 September 2015)

The development of high performance computing facilities makes possible a massive production of nuclear data in a full microscopic framework. Taking advantage of the individual potential calculations of more than 7000 nuclei, a new statistical scission-point model, called SPY, has been developed. It gives access to the absolute available energy at the scission point, which allows the use of a parameter-free microcanonical statistical description to calculate the distributions and the mean values of all fission observables. SPY uses the richness of microscopy in a rather simple theoretical framework, without any parameter except the scission-point definition, to draw clear answers based on perfect knowledge of the ingredients involved in the model, with very limited computing cost.

DOI: 10.1103/PhysRevC.92.034617 PACS number(s): 24.75.+i, 25.85.−w, 27.80.+w

I. INTRODUCTION

"A satisfactory theoretical interpretation of the asymmetric mass distribution observed in nuclear fission at low excitation energies has been sought since the discovery of this complex nuclear reaction." With this affirmation begins one of the major reference papers on the interpretation of the fission process, published in 1976 by Wilkins, Steinberg, and Chasman [1], and it is still relevant forty years later despite a huge theoretical and experimental effort. So what makes this physics process so difficult to describe?

A proper fission reaction description faces all the difficulties associated with theories describing the atomic nucleus. This phenomenon only occurs for rather heavy nuclei for which an exact quantum description of the many-body problem is out of reach. However, several recent models seek to provide a detailed description based on mean-field [2] and macro-microscopic approaches [3–5]. It is not yet possible to provide an exact description of the system by quantum thermodynamics given the lack of knowledge on the partition of numerous degrees of freedom involved during the system evolution. In addition, they all require significant computing time.

Together with theoretical developments, many experiments have been performed since the 1980s to explore new fissioning systems, from exotic light nuclei within the lead region [6], up to new superheavy nuclei [7,8]. In addition, a very rich set of data on the charge yields has been measured from lead to uranium in inverse kinematics [9]. Taken together, these data highlight a transition from symmetric fission for proton-rich nuclei to asymmetric fission for neutron-rich nuclei. Understanding the origin of this transition requires a fission model based on a coherent theoretical framework applicable to the entire nuclei chart.

A new theoretical approach, based on a statistical modeling of the scission point, has been developed using a microscopic description of the fragment nuclear structure. These microscopic ingredients [10] are calculated with the Gogny interaction [11]. Therefore, this approach is complementary with the historical mean-fields theories based on the same interaction [2].

This new model, called SPY (scission-point yield), is largely inspired by the scission-point model originally developed by Wilkins *et al.* However, there are reasons pointing to a need for a renewal of historical formalism. First, major theoretical advances in nuclear structure description have been made since the late 1970s and they have never been included in an updated version of the Wilkins model. Second, a predictive and fast model is useful to generate nuclear data to study the fission process over a large range of nuclei, from light nuclei such as mercury to heavy ones like fermium. This is why the SPY model has been developed: it is capable of making reasonable predictions for every fissionable nucleus, while achieving very moderate computation cost. This makes it very appealing for several applications, in particular astrophysics calculations [12]. Finally, a statistical description of the scission point that is as complete as possible allows for the estimation of effects which are not included in the model, especially coming from the system dynamics, and for an assessment of the sensitivity to the reaction entrance channel. This model will favor discussions on experimental results interpretation.

As mentioned by Wilkins, "the principal aim is to investigate the general validity and applicability of our model and not to attempt to achieve the optimum fit to the experimental data for each fissioning system." The SPY model has been

*Former member of the laboratory.

developed keeping the same spirit and no adjustments to any data have been done.

II. THE SPY MODEL

SPY is a renewed version of the well-known scission-point model developed by Wilkins *et al.* [1] in the late 1970s. It is based on the basic assumption that the gross properties of the fission fragment distributions can be determined from the available energy of the different configurations at the scission point. Assuming a thermodynamic equilibrium at scission, a statistical treatment can be used to calculate the fission fragments' distributions. The model is based on two pillars: the definition of the scission point (Sec. II A), on the one hand, and the calculation of the absolute available energy for each configuration (Sec. II B) allowing the statistical description (Sec. II C), on the other.

A. The scission-point definition

During the fission process, the system evolves from a quasispherical or slightly deformed compound nucleus to two fragments flying away from one another due to their Coulomb repulsion. The dynamical evolution of the system presents two characteristic points: the outer saddle point and the scission point. The first is defined as the configuration where the fission of the system is inevitable and it is clearly defined by a topological criterion on the potential energy surface of the fissioning system. After the saddle point the system continues to deform; a neck appears and becomes more and more thin until breaking, giving rise to two fragments. The scission point, somewhere between the saddle point and the two separated fragments far apart, is difficult to define unambiguously. At scission, the nuclear density in the neck region between the nascent fragments may be considered as vanishing, and the wave function of any nucleon spreads over each of the fragments. In this configuration, all fragments properties (mass, charge, and deformation) can therefore be considered as fixed. Nevertheless, the scission configuration presents an ambiguous topological definition, and different criteria have been used for its identification. In particular, in several microscopic approaches (see for example [2,13]) the scission configuration is identified by energy criteria, i.e., the sudden drop of the total binding energy, or according to the ratio between the nuclear interaction and the Coulomb repulsion between fragments [14]. In all cases, the scission configuration topology depends on the chosen criteria, and, contrary to what Wilkins et al. stated, scission can hardly be defined by the sole distance between the two fragments. Nevertheless, the potential energy surface (PES) of the system, calculated through a self-consistent Hartree-Fock-Bogoliubov (HFB) formalism, is rather smooth between the saddle point and the scission point, at least for major actinides, and the nuclear matter density extracted near the scission line gives a scission distance ranging from 3 to 7 fm [2,15].

Therefore, as in Wilkins's work, the system at scission is modeled by two coaxial nuclei separated by a fixed distance, and the fragment shape is described by quadrupole deformations. This simple but realistic first-order description of the nuclear deformation of the fragments allows for reliable calculations of the energy of the system, and more importantly can be unambiguously connected to the HFB potential energies of the nuclei. Given this definition of the scission configuration, each nucleus is characterized by its neutron and proton numbers (N,Z) and its deformation parameter $(\tilde{q})$.

A fixed scission distance of 5 fm is used in all calculations presented in this work. It ensures that the quadrupole shape family used for the scission description is relevant and somehow corresponds to a first-order optimum as discussed in [16]. The chosen value is different from the initial choice of Wilkins who considered a distance of 1.4 fm, based on the range of the strong interaction. The influence of this choice on the energy balance at scission has already been discussed in [16] and will be further discussed in this work.

B. The energy balance at scission

Once a system configuration at scission is defined, the first stage of the SPY model consists of achieving detailed energy balance for all possible fragmentations (around 1000 for actinide fission) as a function of the deformation parameter of the two fragments. The available energy (E_A) is calculated as the difference between the scission potential energy of the system composed by the two nascent fragments in interaction and the excited compound nucleus energy (E_{CN}):

$$\begin{aligned} E_A = {} & E_{\rm ind}(Z_1,N_1,\tilde{q}_1) + E_{\rm ind}(Z_2,N_2,\tilde{q}_2) \\ & + E_{\rm coul}(Z_1,N_1,\tilde{q}_1,Z_2,N_2,\tilde{q}_2,d) \\ & + E_{\rm nucl}(Z_1,N_1,\tilde{q}_1,Z_2,N_2,\tilde{q}_2) \\ & - E_{CN}. \end{aligned} \tag{1}$$

The scission potential energy is obtained as the sum of

(i) The individual energy for each of the two fragments $(E_{\rm ind})$, which is a function of their deformation.
(ii) The interaction energy between the fragments, described as the sum of a Coulomb repulsion term $(E_{\rm coul})$ and a nuclear interaction term $(E_{\rm nucl})$. The interaction energy depends on the deformation parameters of the fission fragments and on their distance.

As a consequence, a given configuration is energetically reachable only if the available energy of the system at scission is lower than the total energy of the compound nucleus. In other words, a scission configuration is possible only if $E_A < 0$. By convenience, the absolute value of the available energy will be used thereafter and only energetically reachable scission configurations will be taken into account.

A prescission kinetic energy could be taken into account and would modify this equation. Since there is no proper well-defined formalism to introduce it and it depends on the scission point definition, this energy is not taken into account.

The axial symmetry of the compound nucleus is supposed to be conserved in the system formed by the two fragments. Moreover, the scission potential energy depends rather weakly on high-order deformations, typically higher than the quadrupole momentum. Therefore, the deformation parameter used in the SPY model only accounts for quadrupole deformation, i.e., elongation. The compound nucleus energy

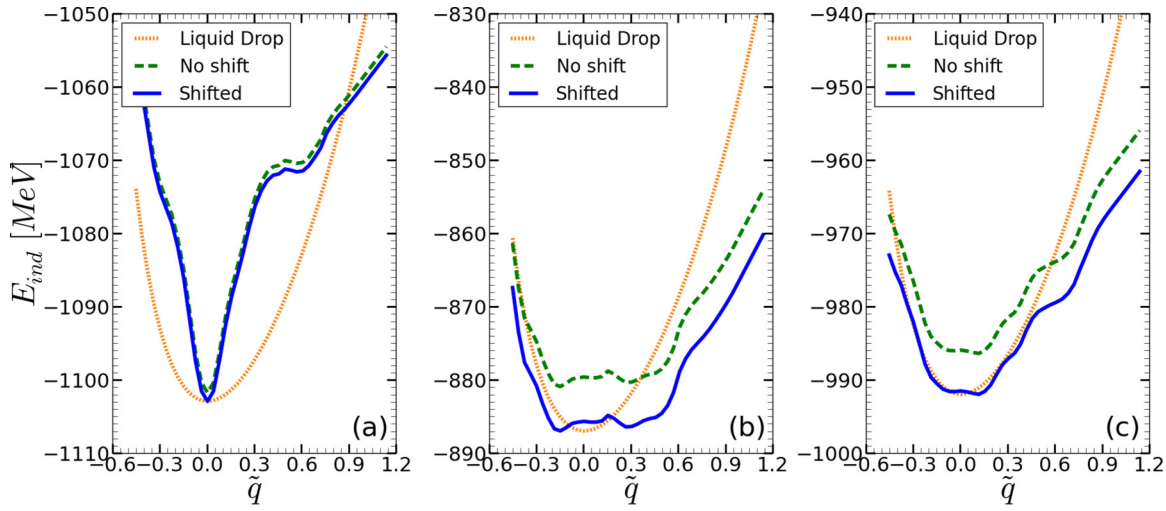

FIG. 1. (Color online) Liquid drop (orange dotted line), HFB (green dashed line), and shifted HFB (blue solid line) potential energy as a function of deformation for ^{132}Sn (a), ^{104}Mo (b), and ^{118}Pd (c). Liquid drop ground state energy is shifted to HFB ground state energy.

E_{CN} is defined as the sum of the ground state energy of the fissioning nucleus and its excitation energy. The excitation energy depends on the involved reaction (neutron-, proton-, photo-induced or spontaneous fission) and is distributed among all degrees of freedom. The ground state energy of the compound nucleus is taken as its experimental mass (when available) or as a theoretical prediction calculated on the basis of mass systematic [17]. The mass, charge, and excitation energy of the compound nucleus are the only inputs of the model since they totally define the initial condition of the fission reaction. At this stage, SPY does not include any deformation-dependent nuclear structure property or angular momentum of the compound nucleus nor its possible deexcitation prior to fission. This latter constraint restricts the possible comparison with data only to low-energy induced fission.

1. The individual energy

The individual energy (E_{ind}) of each nucleus is derived from an up-to-date microscopic description of its nuclear structure. This potential energy is calculated within the framework of a self-consistent HFB formalism using the Gogny D1S nucleon-nucleon interaction [11]. The HFB equations are solved iteratively by expanding the quasiparticle wave functions in a truncated harmonic oscillator basis under the axial hypothesis where the quadrupole momentum operator is projected into a fixed value (and triaxiality is neglected). The so-called reduced quadrupole momentum ($\tilde{q}$) is linked to the quadrupole momentum (q_{20}) by the relation

$$\tilde{q} = \frac{q_{20}}{AR_0^2} \tag{2}$$

where A is the nuclear mass and R_0 its radius ($R_0 = r_0 A^{1/3}$). The individual energies used in SPY are compiled within the AMEDEE database [10,18] which contains the nucleus' potential energy as a function of its deformation parameter over a large range of deformations, from very oblate ($\tilde{q} = -0.45$) to very prolate shapes ($\tilde{q} = 1.14$), and for all the nuclei of the whole nuclear chart (see for example Fig. 1).

The ground state energy calculated within the HFB formalism is known to differ from the experimental mass. This is mainly due to the mean field approximation and the use of a finite basis in the HFB states expansion [10,19,20]. The difference between the measured mass and the HFB ground state energy can be several MeV, especially in the case of "soft" nuclei where shape coexistence is involved or neutron-rich nuclei. Nevertheless, the predictive power of the microscopic calculations mostly concerns the description of the nuclear structure as a function of the deformation, instead of the absolute value of the potential energy. Therefore, to achieve precise energy balance, the whole HFB potential energy surface (E_{HFB}) is globally shifted so that the ground state energy fits the experimental masses or a theoretical value calculated on the basis of mass systematics (for instance [17]).

The shifted energy, which keeps all relevant microscopic information on the structure evolution with the deformation, is used to perform the energy balance defined in (1). The three examples presented in Fig. 1 show the typical shape of the HFB energy of a nucleus as a function of its deformation. The shift to the actual mass varies from a few keV for magic nuclei up to 10 MeV for midshell nuclei.

The importance of a microscopic description is visible when comparing the HFB energy with a liquid drop potential energy [21,22]. The richness brought by microscopy lies in the natural appearance of shell effects, which will finally influence the available energy for the different fragmentations at scission.

During the descent from saddle to scission, the system could dynamically increase in temperature. At scission, a potential energy calculated in a finite-temperature HFB framework would thus be better adapted. The main impact of the temperature on the potential energy would be a decrease in the nuclear shell and pairing effects. This effect, taken into account by Wilkins *et al.* by an intrinsic temperature-dependent shell correction term, is not taken into account due to the lack of a proper modeling of dissipation from saddle to scission and to to

the absence of temperature-dependant microscopic individual energy. Moreover, the statistical description of a system with a potential energy calculated in a finite-temperature framework must be properly handled in order to avoid double counting of temperature-dependent effects (shell and pairing effects).

The influence of pairing energy on the available energy at scission can be rather large since it is around 2 MeV between an even-even and an odd-odd fission fragment in the case of actinides. This difference is generally quite significant with respect to the energy variation between two successive even nuclei due to shell effects. Therefore, the impact of pairing on fission observables is too strong and, as a first step, it is suppressed by washing the pairing effect on the nuclear masses. In the case of an odd-odd nucleus, its mass is interpolated between the four neighboring even nuclei (the two adjacent proton-even and the two adjacent neutron-even).

2. The interaction energy

The fission fragments at scission are separated by a few fm and are submitted to the nuclear interaction and to the Coulomb repulsion.

The nuclear interaction is determined from the Blocki prescription [23], which mainly depends on the distance between fragment surfaces, the isospin asymmetry of the fissioning nucleus and the fragments curvature along the scission axis. However, since the scission distance of 5 fm is greater than the mean range of nuclear interaction, this term is always below 1 MeV and can be neglected compared to the Coulomb energy that is of the order of 200 MeV. Nevertheless, the nuclear interaction is always included in the calculation for completeness.

The fission fragments are rather close at scission and induce a high Coulomb interaction. Therefore, a proper calculation requires a detailed description of their charge distributions since they cannot be considered as point-like. The charge distribution of a given fragment depends on its proton and mass numbers and on its deformation. In the present version of the SPY model, the fragments are considered as uniformly charged without diffusivity. The nuclear shape is fully described by the quadrupole deformation of an axially symmetric nucleus to ensure the best coherence with respect to the individual HFB energy, which is calculated imposing a constraint (via a Lagrange parameter) on a quadrupolar momentum operator. The nuclear shape is described by a parametrization defined as $R(\theta,\varphi,\alpha_{20})$, where α_{20} is the quadrupole component of the nuclear shape, expanded over a Legendre polynomial basis:

$$R(\theta,\varphi,\alpha_{20}) = R_0\lambda(\alpha_{20})^{-1}\left(1+\alpha_{20}\sqrt{\frac{5}{4\pi}}\frac{3\cos(\theta)^2-1}{2}\right). \tag{3}$$

The coefficient $\lambda(\alpha_{20})$ ensures volume conservation according to the deformation

$$\lambda(\alpha_{20}) = \left(1+\frac{3}{4\pi}{\alpha_{20}}^2+\frac{2}{35}\left(\frac{5}{4\pi}\right)^{3/2}{\alpha_{20}}^3\right)^{1/3}. \tag{4}$$

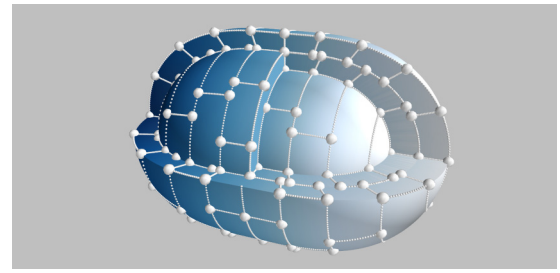

FIG. 2. (Color online) Integration mesh for ^{132}Sn with quadrupole deformation $\tilde{q} = 0.4$. The points and the dotted lines represent vertices and edges of the elementary volumes.

The dimensionless reduced quadrupole momentum, used throughout this work, is defined as

$$\begin{aligned}\tilde{q} &= \frac{2}{A{R_0}^2}\int r^2\rho(\vec{r})\frac{3\cos(\theta)^2-1}{2}d\vec{r}\\ &= \sqrt{\frac{9}{5\pi}}\lambda(\alpha_{20})^{-5}\left(\alpha_{20}+\frac{4}{7}{\alpha_{20}}^2\left(\frac{5}{4\pi}\right)^{1/2}+\frac{6}{7}{\alpha_{20}}^3\frac{5}{4\pi}\right.\\ &\quad\left.+\frac{20}{77}{\alpha_{20}}^4\left(\frac{5}{4\pi}\right)^{3/2}+\frac{53}{1001}{\alpha_{20}}^5\left(\frac{5}{4\pi}\right)^2\right).\end{aligned} \tag{5}$$

At the first order in α_{20}, $\tilde{q} = \sqrt{\frac{9}{5\pi}}\alpha_{20} + o(\alpha_{20})$. The Coulomb interaction energy is then calculated explicitly through numeric integration over the two fragment volume with uniform charge densities $\rho_1 = \frac{Z_1}{V_1}$ and $\rho_2 = \frac{Z_2}{V_2}$:

$$E_{\text{coul}} = \int_{V_1}\int_{V_2}\frac{\rho_1\rho_2}{\|\vec{r}_1-\vec{r}_2\|}d\vec{r}_1 d\vec{r}_2 \tag{6}$$

For the integration, the volume of each fragment is determined by its shape, itself parametrized by its deformation α_{20}. To calculate the Coulomb interaction, an integration mesh needs to be defined for each fragment. Since spherical coordinates (r,θ,φ) are used to define the shape of each fragment, the mesh is also defined in spherical coordinates to avoid numerical errors due to nonconservation of the fragment volume. However, with constant steps in r, θ, and φ, elementary volumes close to the fragment surface are bigger than the inner ones. In order to optimize the computation time, a special mesh is needed. This mesh is conceived to minimize the approximation error by considering elementary cells of similar volumes. The fragment volume is divided into $i_{\max}$ shells of equal thickness and each shell is divided according to θ coordinate. The θ step depends on the shell location and decreases with the shell number. The φ step depends on shell location and θ (see Fig. 2).

For a fixed distance between the surfaces of the two nuclei, the Coulomb energy decreases rapidly while the deformation increases from oblate to prolate shapes (Fig. 3) due to the increasing distance between the two centers of mass.

3. The available energy at scission

The energy balance at scission is calculated from Eq. (1) for all possible fragmentations (around 1000). To reduce

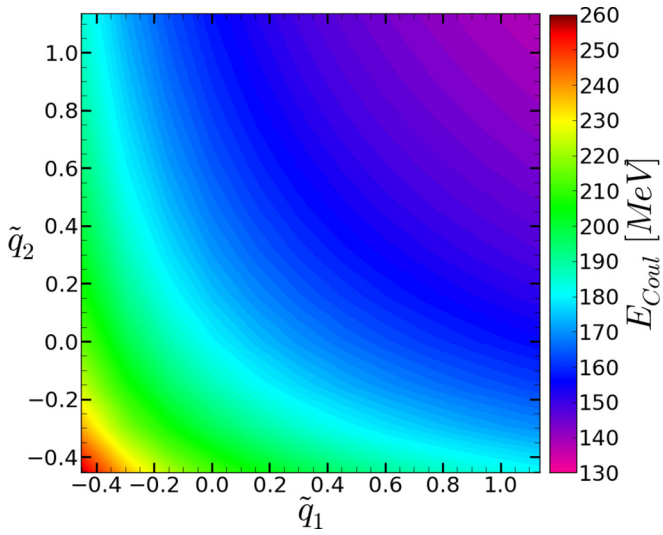

FIG. 3. (Color online) Coulomb energy between two fragments (fragment 1: ^{132}Sn; fragment 2: ^{104}Mo) as a function of their quadrupole deformation.

computational cost, the individual energies are tabulated, leading to a rather small computing time for exploring all possible fragmentations of a fissioning nucleus. As an example, we present the results of the energy balance performed for the thermal neutron-induced fission of ^{235}U. In this case, the excitation energy of the compound nucleus (^{236}U*) is 6.54 MeV. The calculation of the energy balance for all configurations on a single core computer takes around 10 minutes.

Before discussing the potential energy surface of a given fragmentation, we shall outline one preliminary feature. Two opposite effects occur in the available energy balance. On the one hand, the interaction energy decreases regularly from oblate to prolate shapes. On the other hand, the individual energy increases significantly with the fragment deformation far from the ground state. Therefore, two antagonistic effects act as the main drivers of the available energy: the individual energy, which favors ground state deformations, and the interaction energy, which favors prolate shapes.

On the basis of this general trend, the available energy for a given fragmentation reflects the composition of the nuclear structure for each of the two fragments. The available energy of the symmetric splitting (^{118}Pd + ^{118}Pd) is displayed in Fig. 4 and that of the asymmetric splitting (^{132}Sn + ^{104}Mo) is displayed in Fig. 5.

For both fragmentations, the available energy profile is very structured, reflecting the intrinsic energy variations of each nucleus. The available energy maximum for the asymmetric fragmentation (36.5 MeV) is steep, and is found for a spherical ($\tilde{q} = 0$) ^{132}Sn and a largely deformed ($\tilde{q} = 0.45$) ^{104}Mo. In contrast, the corresponding maximum of 28.6 MeV in the symmetric fragmentation is found for a smaller deformation ($\tilde{q} = 0.2$) of ^{118}Pd. The steepness of the energy maximum in the asymmetric fragmentation is due to the doubly magic ^{132}Sn. Therefore, the most energetically favorable fragmentation in thermal neutron-induced fission of ^{235}U is asymmetric due to the nuclear structure of nuclei around ^{132}Sn, compared to the moderated shell effects of soft nuclei around ^{118}Pd.

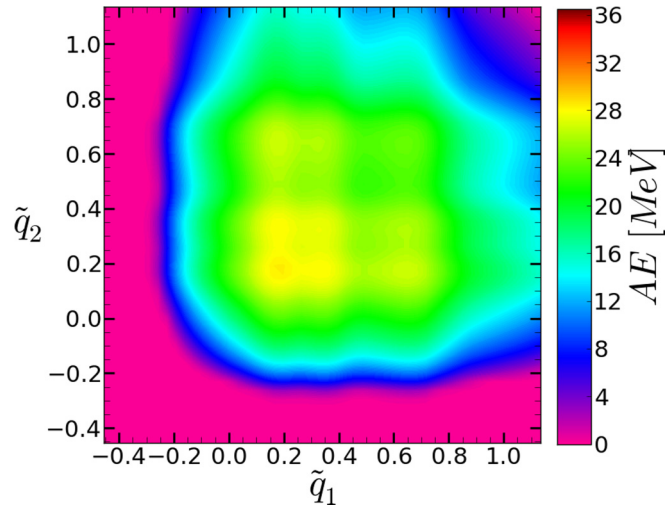

FIG. 4. (Color online) Available energy as a function of the fragments deformation calculated for symmetric (^{118}Pd + ^{118}Pd) fragmentation in the ^{235}U(n_{th}, f) reaction.

The role of shell effects as the main origin of the mass asymmetry is confirmed when looking at the maximum available energy for all possible fragmentations (Fig. 6). The configurations characterized by the largest available energy are favored since, within a statistical interpretation, they give access to the largest phase space. In the case of the thermal neutron-induced fission of ^{235}U, the well-known double-humped structure already appears clearly on the maximum available energy distribution over all fragmentations.

C. A statistical description of scission

In low-energy fission, we assume as Wilkins that a thermal equilibrium is reached at scission. Therefore, the system can be treated as a microcanonical ensemble where all available states of the system are equiprobable.

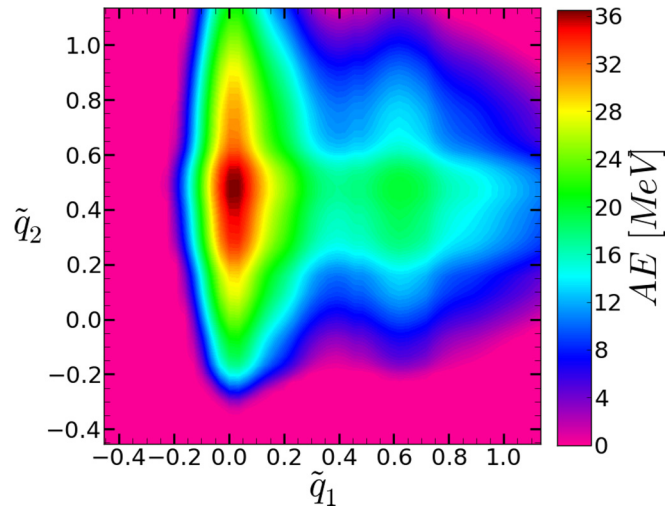

FIG. 5. (Color online) Available energy as a function of the fragments deformation calculated for asymmetric (^{132}Sn + ^{104}Mo) fragmentation in the ^{235}U(n_{th}, f) reaction.

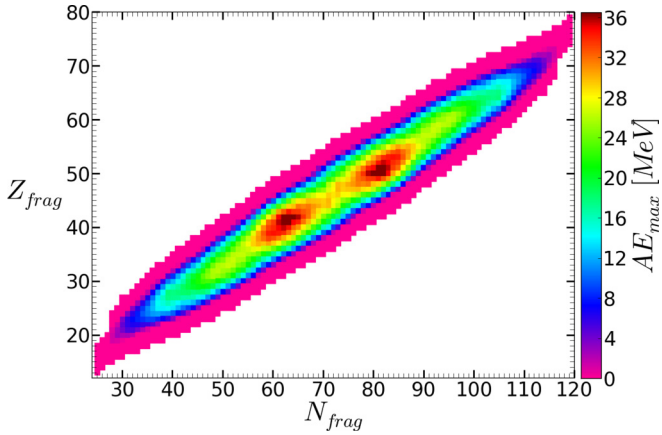

FIG. 6. (Color online) Maximum available energy as a function of the fragment proton and neutron numbers in the ^{235}U(n_{th},f) reaction.

1. The microcanonical description

In this framework, the fission fragment yields can be simply calculated by counting the number of available states at scission for all the different fragmentations. Since the probability for a given fragmentation is related to the available phase space, the knowledge of all exact states is not necessary and only their number for a given configuration is needed. Moreover, each configuration is fully defined by the intrinsic excitation of the two-fragment system as a function of the fragments' deformation. Therefore, only two inputs are required to perform a statistical description of the scission point: the available energy and the state density for each configuration.

The number of available states at scission for a given configuration (π) is assumed to be the product of the state densities of the two isolated fragments (ρ_1 and ρ_2) where a fraction x of the available energy is transferred to fragment 1 while the fraction $(1-x)$ goes to fragment 2:

$$\pi(Z_1,N_1,Z_2,N_2,\tilde{q}_1,\tilde{q}_2,x) = \rho_1(xE_{\text{avail}})\rho_2((1-x)E_{\text{avail}})\delta E^2. \quad (7)$$

Therefore, the probability of a given fragmentation at a given deformation is proportional to π. Finally, the total probability P to obtain a fragmentation is obtained by integrating the number of states π over the two deformation parameters and all energy partitions:

$$P(Z_1,N_1,Z_2,N_2) = \int_{-0.45}^{1.14}\int_{-0.45}^{1.14}\int_{0}^{1} \pi\, dx\, d\tilde{q}_1 d\tilde{q}_2. \quad (8)$$

This probability, normalized to 200%, is the production yield of each fission fragment.

Presently, the calculation of the state density of fission fragments is performed in the framework of a Fermi gas description where the nucleons of a nucleus are considered as a gas of fermions confined in a box. Therefore the state density of a nucleus with intrinsic excitation energy ε is given by [24]

$$\rho(\varepsilon) = \frac{\sqrt{\pi}}{12}\frac{e^{2\sqrt{a\varepsilon}}}{a^{1/4}\varepsilon^{5/4}} \quad (9)$$

This state density is independent of the fragment deformation and only depends on the level density parameter a. In the framework of a Fermi gas model, where only single-particle states are considered, the value $a \approx A/13$, where A is the nuclear mass, is usually taken [25]. However, the comparison with experimental data shows that a level density parameter closer to $A/8$ is better adapted [25]. This difference comes from the presence of collective states that are not counted in a Fermi gas model. Therefore, this latter value has been chosen as a basis for the SPY model. However, It is worth mentioning that using $A/13$ instand of $A/8$ has minor impact on the results.

Since statistical treatment using a Fermi gas state density does not introduce any structure effect, the most probable fragmentation will be mainly defined by the highest energy available for the system. Given this statistical description, the mean value of all relevant observables can be calculated. For a given observable X, its mean value $\langle X\rangle$ is obtained as

$$\langle X\rangle = \int X\pi\, dx\, d\tilde{q}_1 d\tilde{q}_2 \quad (10)$$

The three main fission fragment observables that will be studied in this work are the production yields, the kinetic energy, and the excitation energy, this last observable leading to the number of evaporated neutrons. On this topic, the results will be presented and discussed for the thermal fission of ^{235}U. Then these results will be generalized in Sec. III to many other fissioning systems.

2. Yields

The fragment mass and charge yields in the thermal neutron-induced fission of ^{235}U calculated with SPY are presented in Fig. 7. The SPY model does not include any parameter or any adjustment. Since this model is focused on the scission-point description, the neutron evaporation of the fission fragments is not taken into account in the yield distributions.

The calculated yields present a double-humped distribution peaked around mass 132 and 104 and around corresponding charges 50 and 42. This result reflects the predominant effect of the double magic spherical ^{132}Sn whose high steep potential

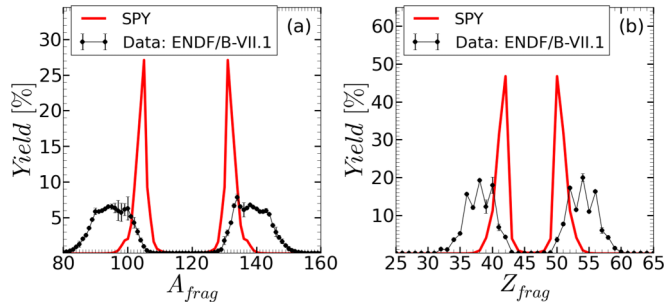

FIG. 7. (Color online) Fragment mass (a) and charge (b) yields in the ^{235}U(n_{th},f) reaction calculated with SPY (in red) compared to evaluated data (post neutron evaporation) from the ENDF/B-VII.1 data library (in black) [26].

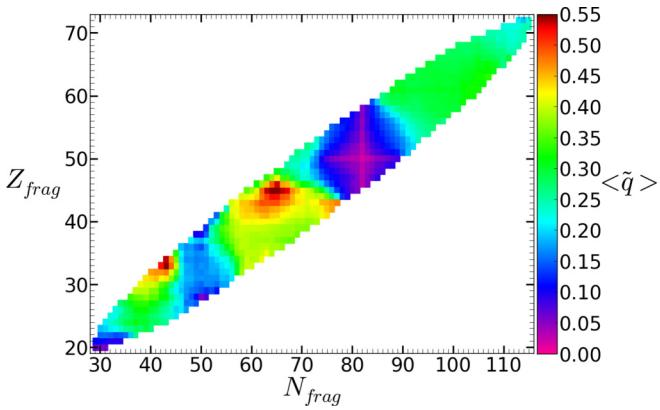

FIG. 8. (Color online) Mean fragment deformation in the ^{235}U(n_{th}, f) reaction.

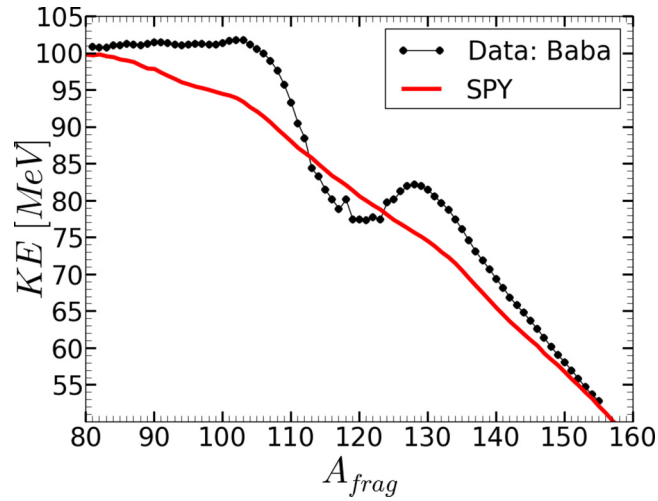

FIG. 9. (Color online) Fission fragment kinetic energy in the ^{235}U(n_{th}, f) reaction calculated with SPY (red line) compared to experimental data from Baba [27] (black line).

provides a very large available energy. Moreover, the soft nucleus ^{104}Mo is very deformed due to Coulomb repulsion, which favors prolate shape. This effect is observed in Fig. 8 where the mean deformation of each fragment is represented. The quadrupole moment varies from 0 (spherical nuclei) up to 0.55 (very prolate nuclei). As expected, oblate shapes are not favored in fission. The symmetric splitting, corresponding to $Z = 46$ and $N = 72$, is disfavored in comparison to configurations involving strong shell effects around ^{132}Sn and its strongly deformed ($\tilde{q} > 0.3$) partner.

Coming back to the fission fragment yields (Fig. 7), the mass and charge yields calculated with SPY are compared to the evaluated data from the ENDF/B-VII.1 library [26]. The experimental distributions are wider than the SPY predictions and span over larger mass and charge ranges. This difference, already observed and discussed by Wilkins *et al.*, is due to two main effects: first, the overestimated impact of shell effects makes double magic nuclei largely favored since they act as an "attractor" for most fragmentations. Second, the use of a Fermi gas state density amplifies this effect due to its exponential behavior with excitation energy.

3. Mean kinetic energy

The kinetic energy of fission fragments is essentially provided by the Coulomb repulsive interaction between the two charged nuclei. Therefore, the importance of a detailed prediction of the fragment deformation at scission is fundamental in order to provide reasonable predictions on the kinetic energy. The SPY results are presented in Fig. 9, together with the experimental data from [27]. The general trend is correctly reproduced since it is mainly driven by the product $Z_1 \times Z_2$. However, the structures seen in experimental data, which are related to strong structure effects, are strongly attenuated in the SPY results. While structure effects are dominant in the yield distributions, they are nearly absent in the kinetic energy distributions. Although the deformation of fragments is taken into account, its impact on kinetic energy distributions is weak.

4. Mean deformations and neutron evaporation

An experimental observable of great importance in thermal fission is the number of evaporated neutrons for each fragment. As already observed by Wilkins *et al.*, the average fragment deformations and evaporated neutrons [28] display similar behavior as can be seen in Fig. 10.

However, the average number of evaporated neutrons is not only due to fragment deformation. Compared to the conclusions reached by Wilkins *et al.*, the SPY model allows for further investigation into the excitation energy in each fragment and, consequently, into the number of evaporated neutrons. This excitation energy has two components. First, each fragment carries a fraction of the available energy at scission under an intrinsic excitation form. Second, since each fragment could undergo deformation at scission, they have a deformation energy defined as the difference between the potential energy at that given deformation and the energy of the ground state. Indeed, the expected saw-tooth form should emerge from the combination of the intrinsic excitation energy and the deformation energy.

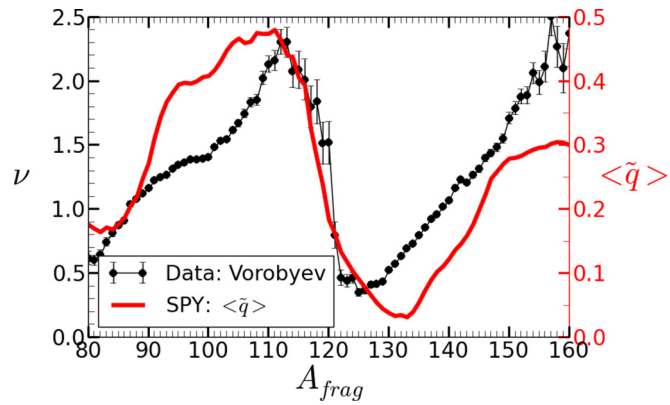

FIG. 10. (Color online) Mean fragment deformation calculated with SPY (red, right scale) in the ^{235}U(n_{th}, f) reaction, compared to the experimental mean number of evaporated neutrons ν (black, left scale) from Vorobyev [28].

A neutron evaporation model could then be used to calculate the number of evaporated neutrons. Since the SPY model only concentrates on the scission phase, the coupling to such a model has not been performed yet. However, as long as the process is energetically possible, we consider that the fission fragments are sequentially deexcited by neutron evaporation. The kinetic energy of evaporated neutrons is randomly taken from theoretical neutron energy spectra (Eq. (7) from [29]) where the temperature of energy spectra depends on excitation energy of fragment (Eq. (5) from [29]). Although the deexcitation cascade of each fragment is not modeled, a mean number of evaporated neutrons could be calculated within this simplified approach and compared to experimental data. The mean number of evaporated neutrons by one fragment in the thermal fission of ^{235}U is estimated at $\overline{\nu} = 2.07$ whereas the experimental total $\overline{\nu} = 2.4$ [30].

D. Impact of different parameters and theoretical choices

Although the SPY model has only one parameter associated with the definition of the scission point, multiple choices on the model ingredients have been made within its development. First, the impact of the scission-point definition will be discussed. Then, the effect of the major choices made within the development of SPY will be presented.

1. On the choice of the scission-point distance

The value of the scission-point distance used in the calculation has a direct and rather trivial first impact on the available energy. The Coulomb energy increases inversely with the distance; i.e. a shorter distance reduces the available energy and increases the kinetic energy of the fragments (Figs. 11 and 12).

However, the scission distance has a lower impact on the fission yields since it only modifies the peak-to-valley ratio without significantly changing the peak position or the maximum yield.

Moreover, second-order effects are more subtle and rather unpredictable because they depend on the sensitivity to the nuclear structure.

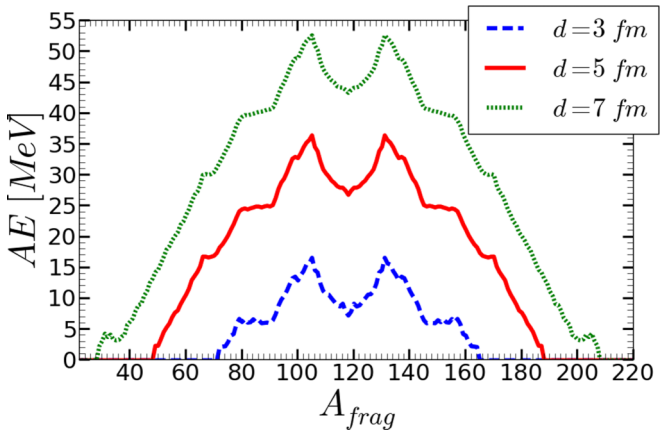

FIG. 11. (Color online) Mean available energy as a function of the fragment mass for different scission distances in the ^{235}U(n_{th}, f) reaction.

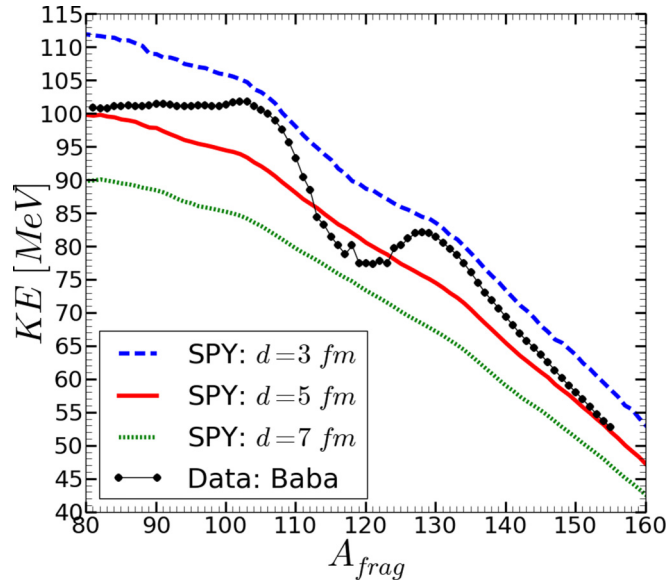

FIG. 12. (Color online) Fragment kinetic energy for different scission distances in the ^{235}U(n_{th}, f) reaction calculated with SPY, compared to experimental data from Baba [27] (black line).

Finally, an increase in sensitivity to the kinetic energy can be observed at short distances by the appearance of small structure effects (Fig. 12). In particular, at a distance of 3 fm, a bump appears in the region of 100–140 mass, similar to that observed experimentally. Moreover, the same tendency is obtained for the number of evaporated neutrons. A decrease in distance leads to lower excitation energy and, consequently, to increased sensitivity to the structure of the fragments.

2. On the statistical ensemble description

The SPY model is based on an absolute energy balance at scission, thus allowing a microcanonical description where the Wilkins model and its relative approach are limited to a canonical one. The results of the two approaches have been compared (Fig. 13).

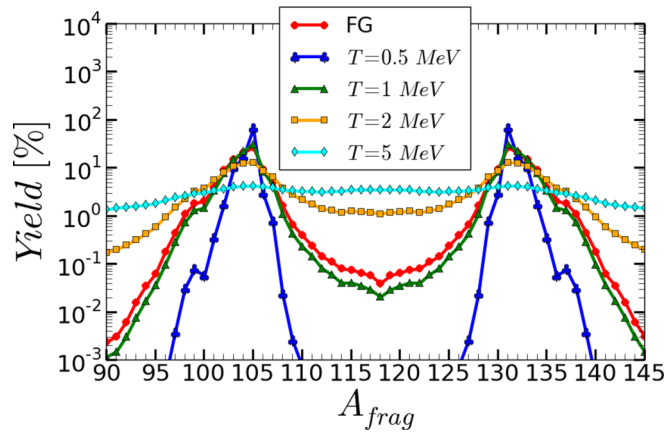

FIG. 13. (Color online) Fragment mass yields in the ^{235}U(n_{th}, f) reaction calculated within the canonical framework at different temperatures and compared to the microcanonical description.

In the canonical description, the probability of a given fragmentation is proportional to the Boltzmann factor e^{-E_A/k_BT}, where T is the temperature of the system. By changing this temperature in the canonical approach, the mass yield distribution could shift from asymmetric at low temperature to symmetric at $T = 5$ MeV (cyan with diamonds curve). SPY predictions based on a microcanonical description are in very good agreement with the canonical description at $T = 1$ MeV, the temperature chosen by Wilkins *et al.* A temperature slightly different of $T = 1.5$ MeV has been chosen in the canonical scission-point model of Ivanyuk *et al.* [31].

E. Evolutions in SPY compared to the Wilkins model

Just like the Wilkins model, SPY is based on the calculation of the energy balance at scission. The use of microscopical potentials is a major improvement in the description of the characteristics of fission fragments up to very exotic nuclei. With the use of a precise double-folding calculation for the Coulomb interaction between the two interacting nuclei, SPY gives access to an absolute value for the available energy at scission with well-defined deformation parameters.

Furthermore, the scission-point starts to have a better definition as we capitalize on advances in theoretical fission modeling and choose it to be within the range conforming to recent microscopic results [2,15].

The access to the absolute available energy allows changing the thermodynamical description and avoiding the inclusion of any temperature parameter. Indeed, Wilkins introduces two temperatures: an intrinsic one to partially wash out the nuclear structure effects and a collective one for the canonical description. We chose to avoid any parameter in order to draw clear answers based on perfect knowledge of the ingredients involved in the model. Furthermore, the microcanonical statistical description allows for the calculation of the distributions and the mean values for all observables.

These improvements were made without loss of computational speed. The calculation of a fissioning system takes a few minutes on a quad-core CPU and a systematic on 3000 fissioning systems takes around one day on a supercomputer using a few tens of CPUs.

III. DISCUSSION ON SEVERAL SPY PREDICTIONS

The model was presented, followed by discussion of the results on the thermal fission of ^{235}U. SPY can now be applied and tested on other fissioning systems. We begin with experimentally known systematics such as the thermal fission of actinides, and then extend the calculations to increasingly exotic systems, up to predictions concerning many nuclei from ytterbium ($Z = 70$) to meitnerium ($Z = 109$), from the proton to the neutron drip line.

A. Fission systematics

After the comparison of the SPY results with experimental data for the thermal fission of uranium, we can generalize to other actinides (Fig. 14). One important feature one can observe is the experimental mass stability of the heavy peak around 140 that is a strong argument for considering

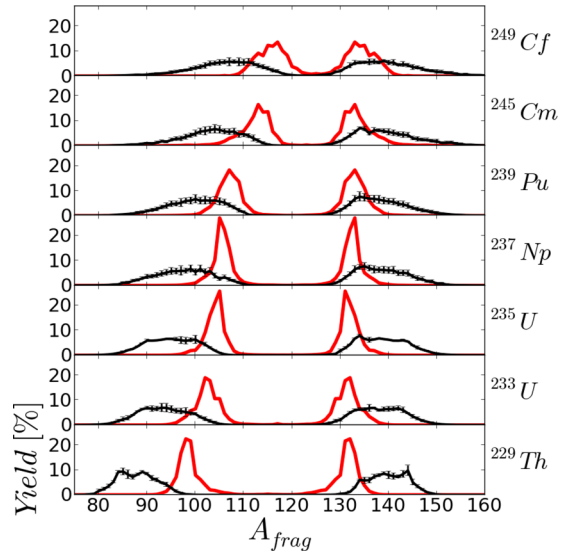

FIG. 14. (Color online) Mass yields in the thermal neutron-induced fission of different actinides calculated with SPY (in red) and compared to evaluated data from the ENDF/B-VII.1 data library [26].

the scission point as a key point for the mass and energy distributions due to the high sensitivity to the structure of the nascent fragments.

The SPY model results present a stability for the heavy peak of the mass distribution around $A = 132$ due to the spherical shell closure. Also, the drawbacks observed and discussed for uraniumare still present for the others actinides: the theoretical heavy peak remains different from the experimental one located at 140, and the width of the theoretical distribution is much narrower. The nuclear structure sensitivity of the SPY model and of the scission-point model in general is too high in the present formalism. To partially solve this problem, Wilkins *et al.* changed the shell correction for ^{132}Sn, introducing a temperature dependence to partially wash out too strong microscopic effects.

Another transition from asymmetric to symmetric charge distributions has been observed for light actinides in Coulomb-induced fission [9] (Fig. 15). SPY globally reproduces this transition, even though it is again shifted by one or two charge units. Beyond a satisfactory qualitative reproduction of existing data, SPY is likely to make predictions when the daughter nuclei exist and are available in the AMEDEE database.

As mentioned, throughout the mass-distribution systematic, the widths are much too narrow by a factor of around 2. Where is the hidden part of the widths? The introduction of a more sophisticated state density could improve the reproduction and, at the same time, reduce the sensitivity to the structure of the fragments included in the HFB individual potentials. Moreover, the absence of dynamic treatment of the fission process can have an impact on the distribution widths.

The width anomaly has a limited impact on energy distributions. The mean total kinetic energy is calculated for all known fissioning systems (red) and compared to the experimental

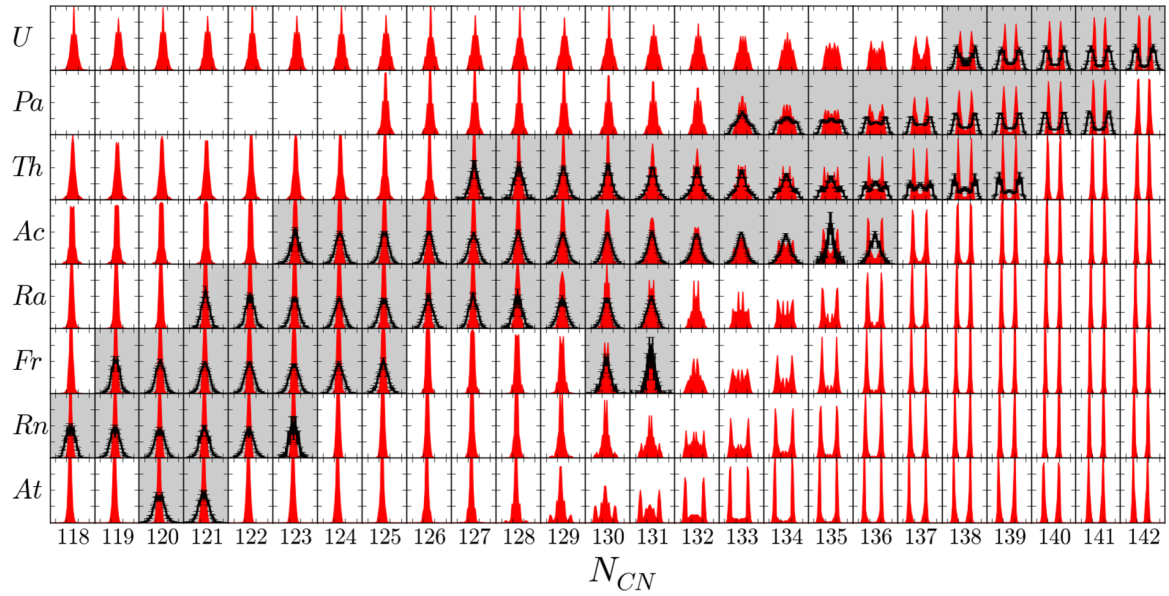

FIG. 15. (Color online) Charge yields for the fission of light actinides region calculated with SPY (in red) compared to data from Schmidt [9] (in black).

results (black) (Fig. 16). A reasonable agreement is achieved for nuclei that present an asymmetric mass-distribution. The results are also compared to the Viola formula [32]. The spread of the experimental points is of the same order of magnitude as the SPY ones. The anomaly on the total kinetic energy (TKE) around 235 MeV for two fermium isotopes and a mendelevium isotope, well above the systematic, is correlated to the preferred formation of two spherical fragments of the same mass. The effect is predicted by SPY but with much weaker amplitude.

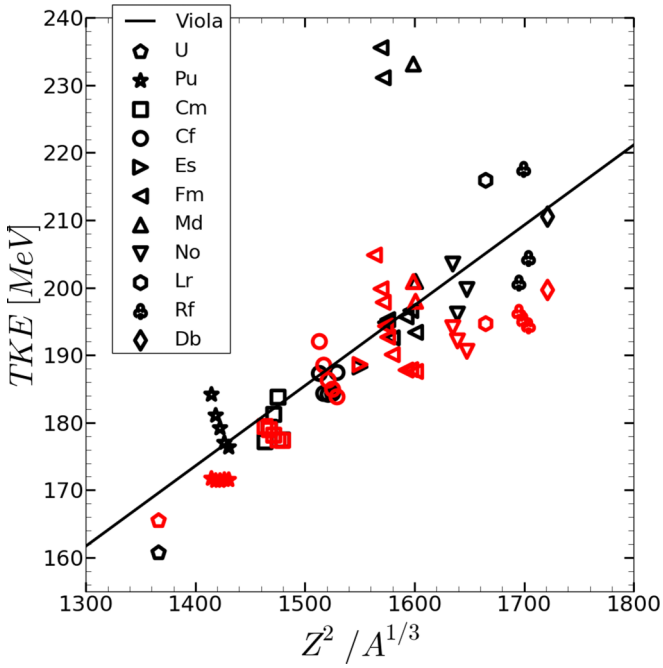

FIG. 16. (Color online) Mean kinetic energy as a function of the compound nucleus fissility calculated with SPY (in red) compared to experimental data [33] (in black) and to the Viola formula [32] (black line).

The SPY model presents satisfactory results to estimate the main variables linked to the last stage of the fission process, without any adjustable parameter. It allows us to find all the major trends of the low-energy fission observables. Therefore, with good confidence, it can be used in areas of the nuclear chart for which there is no experimental result, at least from a qualitative point of view, in particular with respect to the asymmetric or symmetric feature of the fission fragment distributions.

B. Up to exotic nuclei

This study has been generalized to all known and unknown nuclei from ytterbium to superheavy elements (Fig. 17). A peak analysis has been performed for each mass distribution in order to extract the peak multiplicity. This simple procedure allows identifying the zone of transition between symmetric distributions with one peak (yellow), asymmetric ones with two peaks (green) and some exotic distributions with three

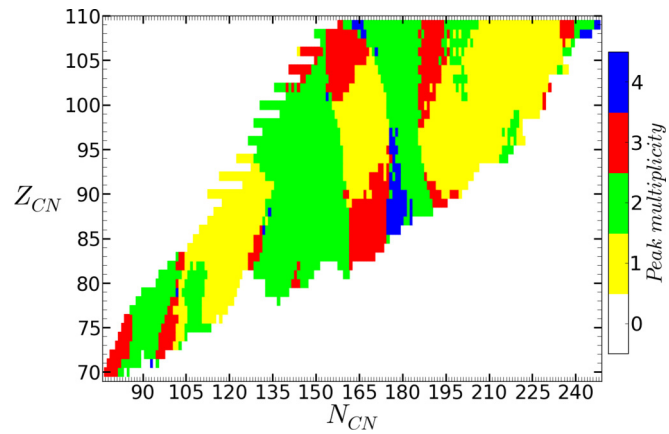

FIG. 17. (Color online) Peak multiplicity in the mass yields as a function of the compound nucleus for an excitation energy of 8 MeV.

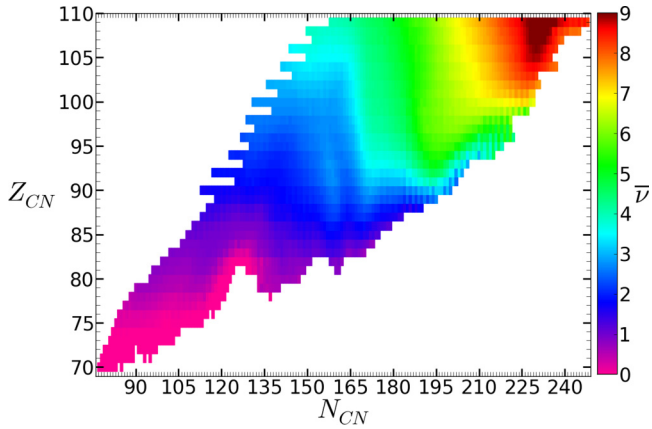

FIG. 18. (Color online) Estimated mean prompt neutron multiplicity per fragment as a function of the compound nucleus for an excitation energy of 8 MeV.

peaks (red), resulting from a symmetric-asymmetric competition, or even four peaks (blue), due to the competition between two asymmetric modes.

The large structures in the peak multiplicity mainly depend on the compound nucleus neutron number inducing mostly vertical structures in Fig. 17. This proves the predominance of the neutron shell closures in the structure of the fission fragment distributions. However, for light nuclei with less than 130 neutrons, the spherical closed neutron shell $N = 50$ does not drive the fission mode as in the fission of ^{180}Hg [16]. In this region, the fission modes are instead driven by deformed shell effects.

The blue area with multiplicity 4 is notable. This doubly asymmetric mode for very neutron-rich nuclei could be the source of the rare-earth production in collapsing neutron stars [12].

The systematic of the total kinetic energy presents a dominant evolution with the proton number of the compound nuclei due to the proton-number dependence of the Coulomb interaction.

The predictions on the excitation energy provided by SPY allows for the systematic calculation of the mean number of evaporated neutrons for each system in the gross approximation explained in Sec. II C 4 (Fig. 18). There are two general dependences. The first one lies in the increasing number of evaporated neutrons for the very neutron-rich nuclei. It has to be correlated with the decreasing separation energy for neutron-rich fragments produced by these nuclei. The second one lies in the general increase in this number with the mass of the compound nuclei. It is simply due to an increase in available energy with the nucleon number of the compound nucleus. This gross evaluation of the number of evaporated neutrons for all existing nuclei has already been used in [12].

IV. CONCLUSIONS AND PERSPECTIVES

Taking advantage of massive calculations to generate a nuclear database including the individual potential of more than 7000 nuclei determined by HFB calculations with the Gogny force, a new statistical scission-point model, called SPY, has been developed. SPY uses the richness and high predictive power of microscopy in a rather simple theoretical framework, leading to the prediction of the most important fission fragment properties, over a huge range of fissioning systems with a very limited computing cost. The model has been presented starting with the careful absolute calculation of the energy available at scission followed by the statistical description used to calculate the major observables associated with the fission fragments.

The SPY results have been compared to the observables measured in the thermal fission of ^{235}U. Since SPY is based on an absolute calculation of the energy available at the scission point, a rather satisfactory reproduction of the evolution of the total kinetic energy is obtained. The absolute available energies are used in a microcanonical description to determine the probability of all possible fragmentations. The general trend of the yield and the mean number of evaporated neutrons are qualitatively reproduced taking into account the absence of any adjustment in the modelization of such a complex process.

The model has been compared with various experimental systematics. In particular, SPY is able to reproduce the general trend of the mass and charge yields transition from asymmetry to symmetry and explains the stability of the heavy peak in the asymmetric regions. Moreover, the model allows for rather satisfactory reproduction of the experimental total kinetic energies. Finally, the model has also been used with success to interpret the fission of exotic mercury isotopes [16] and to predict fission yields for nuclei involved in the coalescence of neutron stars [12].

The model could be enriched in order to study its limits. The width of the mass distribution is too narrow and a shift of a few masses is present between the observed and predicted peak positions. The actual definition of the scission point is proven to be very efficient in performing the calculations but may be criticized due to its simplicity. However, we now have access to full microscopic calculations close to scission, which are actually generalized to all nuclei. They could lead to a better definition of the scission point. In particular, the actual statistical description is based on the basic assumption that the system state density at scission is the product of the state densities of the two nuclei. It has to be verified in the specific microscopical study of the scission point.

Furthermore, the Fermi gas state density is a poor approximation of the real nuclear one. It should be replaced by a microscopic state density calculated in the same framework as the individual potentials. The microscopical effects induced by realistic nuclear densities, will partially counterbalance the structural effects (shell closure and pairing effects) induced by the individual potential. This development of state density calculations for all nuclear deformations and over the whole nuclear chart is a major challenge that will specifically interest the nuclear reaction community, no matter how time-consuming this may seem [34].

ACKNOWLEDGMENT

The authors acknowledge the support and the framework of the COPHYNU (COllaboration between NUclear PHYsics divisions of CEA), within which this work was performed.

[1] B. D. Wilkins, E. P. Steinberg, and R. R. Chasman, Phys. Rev. C **14**, 1832 (1976).
[2] H. Goutte, J. F. Berger, P. Casoli, and D. Gogny, Phys. Rev. C **71**, 024316 (2005).
[3] P. Moller, D. G. Madland, A. J. Sierk, and A. Iwamoto, Nature (London) **409**, 785 (2001).
[4] M. Warda, A. Staszczak, and W. Nazarewicz, Phys. Rev. C **86**, 024601 (2012).
[5] K.-H. Schmidt, B. Jurado, and C. Amouroux, NEA JEFF Report 24, 2014 (unpublished).
[6] A. N. Andreyev, J. Elseviers, M. Huyse, P. Van Duppen, S. Antalic, A. Barzakh, N. Bree, T. E. Cocolios, V. F. Comas, J. Diriken *et al.*, Phys. Rev. Lett. **105**, 252502 (2010).
[7] Y. T. Oganessian, F. S. Abdullin, P. D. Bailey, D. E. Benker, M. E. Bennett, S. N. Dmitriev, J. G. Ezold, J. H. Hamilton, R. A. Henderson, M. G. Itkis *et al.*, Phys. Rev. Lett. **104**, 142502 (2010).
[8] Y. T. Oganessian, F. S. Abdullin, S. N. Dmitriev, J. M. Gostic, J. H. Hamilton, R. A. Henderson, M. G. Itkis, K. J. Moody, A. N. Polyakov, A. V. Ramayya *et al.*, Phys. Rev. Lett. **108**, 022502 (2012).
[9] K.-H. Schmidt, S. Steinhauser, C. Bockstiegel, A. Grewe, A. Heinz, A. Junghans, J. Benlliure, H.-G. Clerc, M. de Jong, J. Muller *et al.*, Nucl. Phys. A **665**, 221 (2000).
[10] S. Hilaire and M. Girod, Eur. Phys. J. A **33**, 237 (2007).
[11] J. Dechargé and D. Gogny, Phys. Rev. C **21**, 1568 (1980).
[12] S. Goriely, J.-L. Sida, J.-F. Lemaître, S. Panebianco, N. Dubray, S. Hilaire, A. Bauswein, and H.-T. Janka, Phys. Rev. Lett. **111**, 242502 (2013).
[13] W. Younes and D. Gogny, Phys. Rev. Lett. **107**, 132501 (2011).
[14] L. Bonneau, P. Quentin, and I. N. Mikhailov, Phys. Rev. C **75**, 064313 (2007).
[15] N. Dubray, H. Goutte, and J.-P. Delaroche, Phys. Rev. C **77**, 014310 (2008).
[16] S. Panebianco, J.-L. Sida, H. Goutte, J.-F. Lemaître, N. Dubray, and S. Hilaire, Phys. Rev. C **86**, 064601 (2012).
[17] P. Moller, J. Nix, W. Myers, and W. Swiatecki, At. Data .Nucl. Data Tables **59**, 185 (1995).
[18] http://www-phynu.cea.fr/HFB-Gogny.htm.
[19] T. R. Rodríguez, A. Arzhanov, and G. Martínez-Pinedo, Phys. Rev. C **91**, 044315 (2015).
[20] S. Goriely, S. Hilaire, M. Girod, and S. Péru, Phys. Rev. Lett. **102**, 242501 (2009).
[21] K. Krane, *Introductory Nuclear Physics* (Wiley, New York, 1988).
[22] R. Hasse and W. Myers, *Geometrical Relationships of Macroscopic Nuclear Physics*, Springer Series in Nuclear and Particle Physics (Springer-Verlag, Berlin, 1988).
[23] J. Blocki, J. Randrup, W. Swiatecki, and C. Tsang, Ann. Phys. (N.Y.) **105**, 427 (1977).
[24] H. A. Bethe, Phys. Rev. **50**, 332 (1936).
[25] J. Toke and W. Swiatecki, Nucl. Phys. A **372**, 141 (1981).
[26] M. Chadwick, M. Herman, P. Obloinsk, M. Dunn, Y. Danon, A. Kahler, D. Smith, B. Pritychenko, G. Arbanas, R. Arcilla *et al.*, Nucl. Data Sheets **112**, 2887 (2011), special issue on the ENDF/B-VII.1 library.
[27] H. Baba, T. Saito, N. Takahashi, A. Yokoyama, T. Miyauchi, S. Mori, D. Yano, T. Hakoda, K. Takamiya, K. Nakanishi *et al.*, J. Nucl. Sci. Technol. **34**, 871 (1997).
[28] A. S. Vorobyev, O. A. Shcherbakov, A. M. Gagarski, G. V. Val'ski, and G. A. Petrov, EPJ Web Conf. **8**, 03004 (2010).
[29] T. Kawano, P. Talou, I. Stetcu, and M. Chadwick, Nucl. Phys. A **913**, 51 (2013).
[30] L. I. Prokhorova, R. E. Bagdasarov, I. I. Kotukhov, V. G. Nesterov, B. Nurpeisov, G. N. Smirenkin, and Yu. M. Turchin, Atomnaya Energiya **30**, 250 (1971) [Sov. At. Energy **30**, 307 (1971)].
[31] F. A. Ivanyuk, S. Chiba, and Y. Aritomo, Phys. Rev. C **90**, 054607 (2014).
[32] V. E. Viola, K. Kwiatkowski, and M. Walker, Phys. Rev. C **31**, 1550 (1985).
[33] D. C. Hoffman, in *Proceedings of the International Conference on Actinides, Santa Fe, New Mexico*, September 1993 [J. Alloys Compd. **213–214**, 67 (1994)].
[34] J.-F. Lemaître, S. Hilaire, S. Panebianco, and J.-L. Sida, Acta Phys. Pol. B **46**, 585 (2015).